Synthesis, Characterization, and Photophysical, Electrochemical, Electroluminescent, and Photovoltaic Properties of Yne-Containing CN−PPVs

Daniel Ayuk Mbi Egbe,*,† Thomas Kietzke,‡ Benjamin Carbonnier,§ David Mühlbacher,|| Hans-Heinrich Hörhold,† Dieter Neher,‡ and Tadeusz Pakula§

Institut für Organische Chemie und Makromolekulare Chemie der Friedrich-Schiller Universität Jena, Humboldstrasse 10, 07743 Jena, Germany, Institute of Physics, University of Potsdam, Am Neuen Palais 10, D-14469 Potsdam, Germany, Max-Planck-Institut für Polymerforschung, Ackermannweg 10, D-55128 Mainz, Germany, and Konarka Austria Forschungs-und-EntwicklungsGmbH, Gruberstrasse 40-42, A-4010 Linz, Austria

Received September 1, 2004; Revised Manuscript Received September 20, 2004

ABSTRACT: Alkoxy-substituted CN-containing phenylene−vinylene−*alt*-phenylene−ethynylene hybrid polymers (CN−PPV−PPE), **3a**, **3b**, and **7a**, were obtained from luminophoric dialdehydes **1** by step growth polymerization via Knoevenagel reaction as high molecular-weight materials. Corresponding CN-free polymers **3c** and **7b** and an ethynylene-free polymer **5** with similar side chains were synthesized for the purpose of comparison. The chemical structures of the polymers were confirmed by IR, ^{1}H and ^{13}C NMR, and elemental analysis. Thermal characterization was conducted by means of thermogravimetric analysis and differential scanning calorimetry. Morphology was investigated by means of optical microscopy and small-angle light scattering. The final morphologies are determined by the molecular characteristics (side chains volume fraction, backbone stiffness) of the studied polymers. All the CN-containing polymers **3b**, **5**, and **7a** exhibit higher fluorescence quantum yield in solid state (50 to 60%), but lower quantum yields (12−40%) in dilute chloroform solution, in total contrast to CN-free polymers **3c**, **3d,** and **7b**. Identical optical, E_g^{opt}, and electrochemical band gap energies, E_g^{ec}, were obtained for **3b**, **3c** and **3d** with intrinsic self-assembly ability, whereas a discrepancy, ΔE_g, was observed in the cases of the fully substituted polymers **5**, **7a**, and **7b**, whose values are dependent on the level of backbone stiffness and length of the side groups combined with the presence or absence of CN units. The incorporation of CN units in **3b** and **7a** lowers their respective LUMO level by 220 and 350 meV compared to their corresponding CN-free counterparts **3c** and **7b**, suggesting an improvement of the electron-accepting strength. Polymers **3b** and **7a** are efficient electron acceptors suitable for photovoltaic application. The experiments indicate that **3b** is a better electron acceptor when used together with M3EH−PPV, but transport properties seem to be better for **7a**. With **3b**, high external quantum efficiencies of up to 23%, an open circuit voltage of up to 1.52 V, and a white light energy efficiency of 0.65% could be realized in bilayer solar cell devices. LED-devices of configuration ITO/PEDOT:PSS/polymer/Ca/Al from **3b**, **3c**, **7a**, and **7b** showed low turn-on voltages between 2 and 2.5 V. The CN-free polymers **3c** and **7b** exhibit far better EL parameters than their corresponding CN containing counterparts **3b** and **7a**.

Introduction

Among conjugated polymers, poly(phenylene−vinylene) (PPV) and its derivatives have been at the center of focus since the first report of electroluminescence from organic polymers in 1990 by the group in Cambridge.[1] This focus was moreover upheaved after the discovery of ultrafast photoinduced femtosecond charge transfer from alkoxy-substituted PPV to the Buckminsterfullerene by Sariciftci and Heeger in 1992.[2] Upon photoexcitation of an electron−hole pair, the transfer of electrons from the polymer onto the fullerene leads to an efficient separation of charges[2,3] (facilitated by a slow microsecond recombination)[4] that is required in photovoltaic devices.[5,6] High electron affinity PPVs are required in the design of high performance light-emitting-diodes[7,8] as well as in organic photovoltaics, where they can act as an electron acceptor component, an alternative to the expensive and poorly soluble fullerene.[9−11] Various methods to enhance the electron affinity of PPVs have been proposed in the literature,[8,12] among which the main method has been the design of CN-substituted PPVs. The CN substituents have been attached either on the double bonds[10,12−17] or on the aromatic rings.[18−19]

Incorporating triple bonds within the PPV backbone, leading to hybrid phenylene−vinylene-*alt*-phenylene−ethynylene polymers (PPV−PPE), as reported recently by Bunz et al., one of us, and others, is one of the recent means to increase the electron uptake of PPVs.[20−24]

The combination of CN units and triple bonds (−C≡C−) within the conjugated backbone of PPVs is expected to provide novel polymers with very high electron-accepting strength to be used in the photovoltaics. This is the subject of this contribution where the synthesis and characterization of CN- and alkoxy-substituted phenylene−vinylene-*alt*-phenylene−ethynylene hybrid polymers **3a, 3b**, and **7a** are presented. While the repeating units (RU) of the partially substituted polymers **3** consist of two −C≡C− units, that of the fully substituted polymer **7a** is made up of one −C≡C− unit, leading to differences in the conjugated

* Corresponding author. Telephone: (+49)-3641−948267. Fax: (+49)-3641−948202. E-mail: c5ayda@uni-jena.de.
† Institut für Organische Chemie und Makromolekulare Chemie der Friedrich-Schiller Universität Jena.
‡ University of Potsdam.
§ Max-Planck-Institut für Polymerforschung.
|| Konarka Austria Forschungs-und-EntwicklungsGmbH.

10.1021/ma048219b CCC: $27.50
Published on Web 11/06/2004

Scheme 1

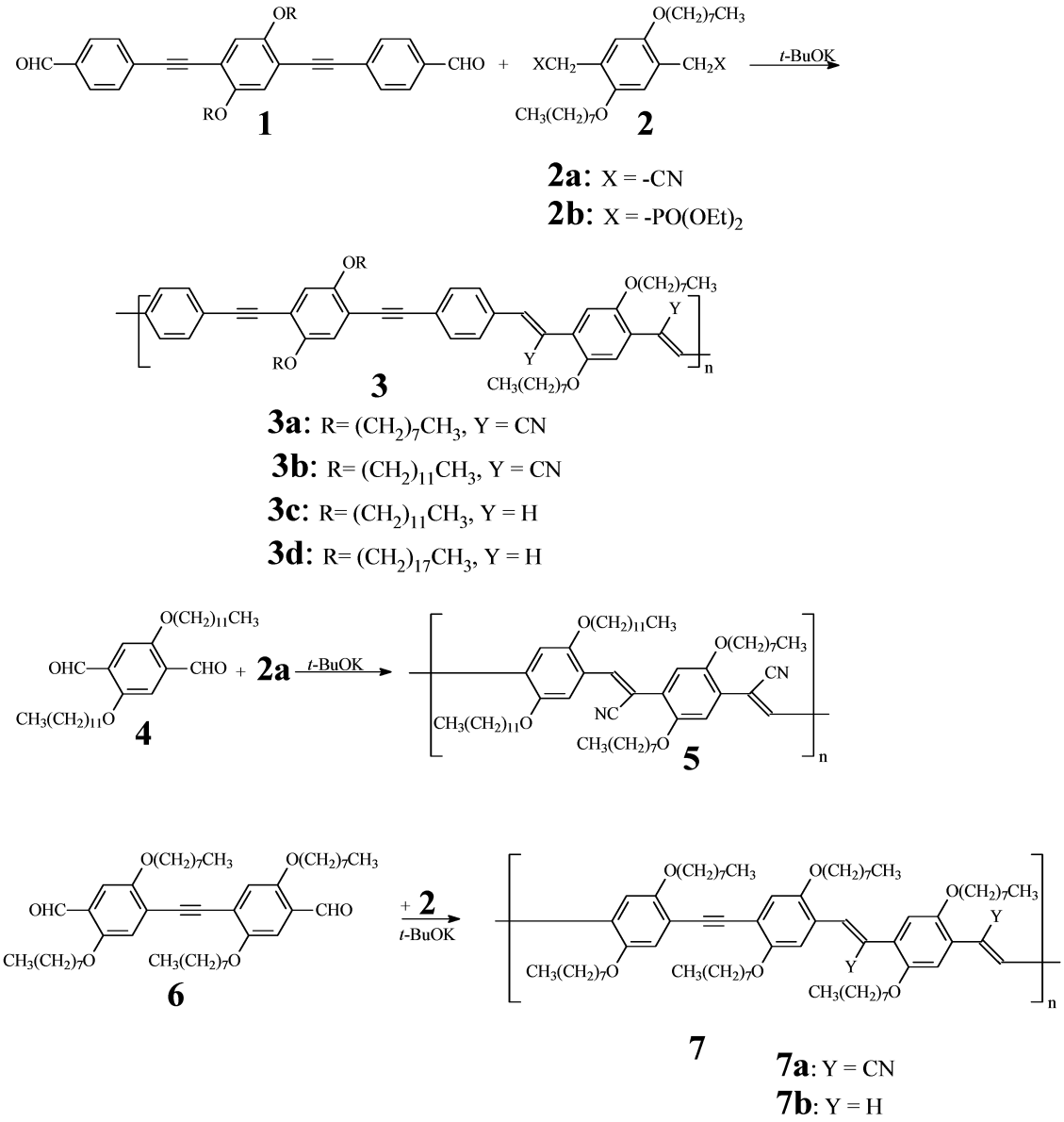

backbone rigidity and consequently to differences in the supramolecular ordering of their thin films.

To fit the energetic scheme of photovoltaic devices it is necessary to determine through electrochemistry the exact energy levels of the valence band (HOMO) and the conduction band (LUMO) and the concomitant width of the gap (known as the electrochemical band gap energy, E_g^{ec}) between the bands of the thin films of the donor and acceptor components.[25] The combination of cyclic voltammetry (CV) and electrochemical voltage spectroscopy (EVS) has proven to be a powerful tool to this effect.[26,27] The energy gap between the bands can also easily be determined through solid film absorption spectroscopy, i.e., optical band gap energy, E_g^{opt}. For the electrochemical investigations, measurements are carried out with *drop casted* films while *spin casted* films are used for devices fabrications and for most of the optical studies, leading to either similarities or differences of the polymer chains alignment (i.e., supramolecular ordering) from both types of preparation methods. This preparation aspect should be taken into consideration while comparing the optical and electrochemical band gap energies.

For the purpose of comparison of the photophysical, electrochemical, and electroluminescent data, CN-free phenylene−ethynylene-*alt*-phenylene−vinylene polymers **3c, 3d**,[21a,22a] and **7b**[24d] and an ethynylene-free CN−PPV **5** were considered. Moreover, results from single layer, blend, and bilayer photovoltaic devices using the above-mentioned polymers are presented and discussed.

Results and Discussion

Synthesis and Characterization. The syntheses of the monomeric dialdehydes **1** [1,4-bis(4-formylphenyl-1-ethynyl)-2,5-dialkoxybenzene],[21a] **6** [1,2-bis(4-formyl-2,5-dioctylphenyl)acetylene],[28] and **2b** [2,5-dioctyloxy-*p*-xylene-bis(diethylphosphonate)][21a] have already been reported elsewhere. 2,5-Dioctyloxy-*p*-xylylenedinitrile (**2a**) was obtained by a three-step synthetic path from hydroquinone as described elsewhere.[15a−b] The synthetic paths to polymers **3a**, **3b**, and **7a** are presented in Scheme 1. They were obtained by a step growth polymerization via Knoevenagel reaction of luminophoric dialdehydes **1** or **6** with dinitrile **2a** in the presence of

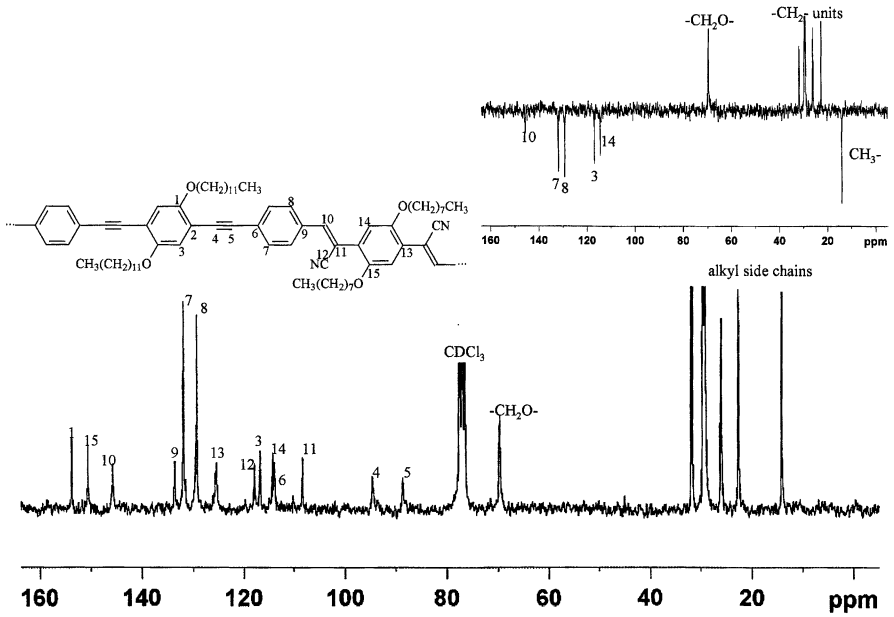

Figure 1. ^{13}C NMR spectrum (100 MHz, $CDCl_3$) of polymer **3b**.

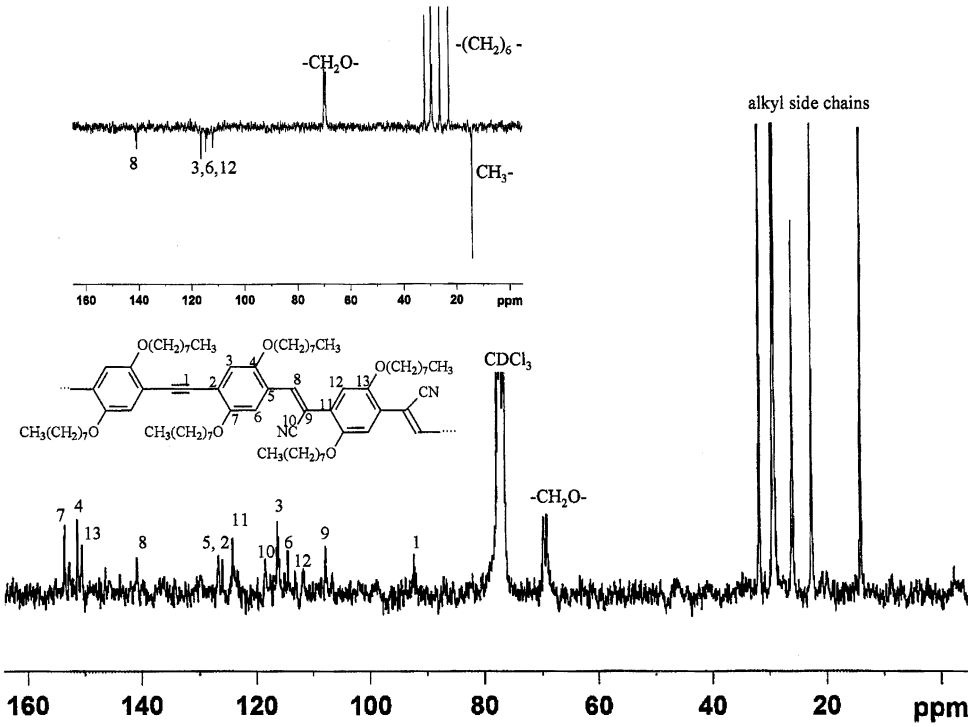

Figure 2. ^{13}C NMR spectrum (100 MHz, $CDCl_3$) of polymer **7a**.

potassium *tert*-butoxide in a mixture of *tert*-butyl alcohol and toluene as solvent. Polymers **3a** and **3b** were obtained as orange fibrous substances in yields of 10% (soluble portion) for **3a** (R = octyl) and 87% for **3b** (R = dodecyl). **7a** was obtained as an orange red compound in 80% yield. Despite the short reaction time (2 h), the main portion of **3a** was insoluble; this can be ascribed to the shorter side chains and high reactivity of this polycondensation method. The soluble portion of **3a** has a number-average molecular weight, $\bar{M}_n$, of 21500 g/mol [degree of polymerization ($\overline{DP}$) = 22] and a polydispersity index (PDI) of 8.4. The highly soluble dodecyl-substituted polymer **3b** and fully substituted polymer **7a** were characterized respectively with a $\bar{M}_n$ value of 35100 g/mol ($\overline{DP}$ = 33, PDI = 3.4) and 39800 g/mol ($\overline{DP}$ = 35, PDI = 2.9). The chemical structures of the polymers were confirmed through NMR, IR, and elemental analysis. Figures 1 and 2 depict respectively the ^{13}C NMR spectra of polymer **3b** and **7a**, measured in $CDCl_3$ (the DEPT spectra are shown as inset). The signals of the acetylenic carbons at 88.7 and 94.7 ppm for **3b** and 92.3 ppm for **7a** and of the vinylene carbons (next to carbons bearing the CN groups) at 145.7 ppm for **3b** and 140.8 ppm for **7a**, among other signals, confirmed the proposed structure of the polymers. Neither aldehyde nor nitrile end groups were detected in NMR and IR spectroscopy. For the purpose of comparison, a CN-free yne-containing PPV, **3c**, and an ethynylene-free CN−PPV, **5**, having similar side chains as **3b**, were also synthesized.

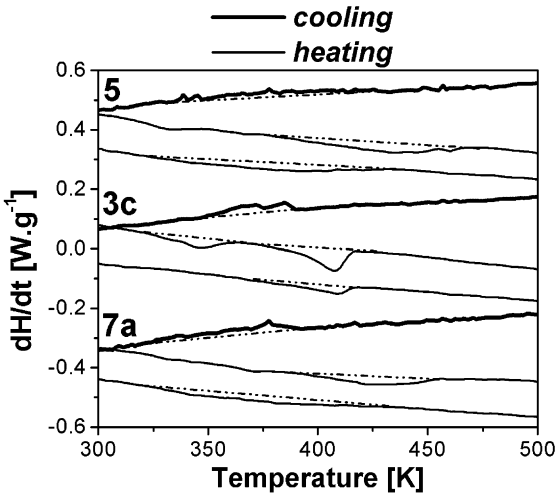

Figure 3. DSC thermograms recorded for bulk sample of **5**, **3c**, and **7a** with the rate 10 K/min. Cooling as well as first and second (bottom) heating runs are shown.

Polymer **3c** was obtained as a yellow material in 71% yield through Horner−Wadsworth−Emmons olefination reaction of dialdehyde **1b** with bisphosphonate ester **2b** based on the synthetic protocol described elsewhere.[21a] This compound is characterized with a $\bar{M}_n$ value of 12000 g/mol ($\overline{DP} = 12$) and a $\bar{M}_w$ value of 37000 g/mol resulting in a polydispersity index of 3.1. Its NMR spectra are similar to those of already reported compounds of the same class.[21a,22a,b] Compound **5**, however, was obtained as a dark red material in 92% yield from the polycondensation reaction of 2,5-didodecyloxyterephthalaldehyde **4** (obtained in a 5-step synthetic route from hydroquinone as described by Chen et al.)[29] with dinitrile **2a** under the same reaction conditions as described above for **3b** and **7a** (Scheme 1). Polymer **5** has a $\bar{M}_n$ value of 8000 g/mol ($\overline{DP} = 9$) and a $\bar{M}_w$ value of 19000 g/mol leading to a polydispersity index of 2.4. The ^{13}C NMR of polymer **5** is given in the Supporting Information as Figure S1. All the peaks could be readily assigned to their corresponding carbons. Both types of end groups were detectable in ^1H NMR, −CHO at 10.44 ppm and $-CH_2CN$ at 3.32 ppm, which is in agreement with the comparatively (to polymer **3b**) lower $\overline{DP}$. Because of the very low yield of soluble portion of **3a**, further investigations were limited to **3b, 3c**, **5**, and **7a**, which are soluble in all common organic solvents.

Thermal Behavior. Thermal degradation measurements, carried out under air while heating at a rate of 10 K/min, showed that polymers **3b**, **3c**, **5**, and **7a** are thermostable at least up to about 623 K, where 5% weight loss was recorded. For **3b**, no distinct first-order transition peaks have been identified in the differential scanning calorimetry runs (not shown here) recorded with the same temperature rate of 10 $K.min^{-1}$. Thermal analysis of **7a** revealed unique melting process in the first heating cycle associated with crystallization recorded in the temperature range 403−303 K. The endothermic process becomes much less intense and appears at lower temperature in the second heating run as presented by the corresponding heating and cooling scans presented in Figure 3. The first heating curve of polymer **5** showed two endothermic peaks around 332 and 434 K, respectively. The higher temperature peak is extended over 100 K. Upon subsequent cooling, an exothermic peak was detected starting from a temperature of 430 K with peak maximum at 378 K, corresponding to the crystallization of **5** upon cooling from isotropic melt as evidenced by polarized optical microscopy (POM). The second heating cycle of **5** revealed one endothermic process with weak intensity occurring in the temperature range between 348 and 428 K. Polymer **3c** exhibits rather similar thermal behavior indicating two endothermic peaks in the first heating run at 345 and 407 K and one melting peak at 408 K in the second heating cycle. The crystallization peak was detected at ∼372 K. However in the case of **3c**, the peaks were observed to be sharpened relative to polymer **5**, suggesting a better defined thermal behavior.

Crystalline Morphologies. In agreement with the DSC analysis, **3b** did not show any phase transition as observed under an optical microscope with crossed polarizers and retained birefringence up to thermal degradation. In contrast to that, **5, 3c**, and **7a** melt into an isotropic liquid at temperatures comparable to those of the high temperature endothermic peaks in the DSC scans. Upon subsequent cooling, speckle patterns were seen at the early stages of crystallization of both polymers showing birefringent compact structures with sizes of the order of few micrometers. However, POM observations did not allow to clearly establish the mechanism of superstructures formation from the isotropic melt. Therefore, morphologies were further investigated using small-angle light scattering technique under cross polarizers. *Hv* SALS patterns presented in the Supporting Information, Figure S2, were recorded at room temperature for **5** and **3c**. They both exhibit a 4-fold symmetry but differ in the orientation of the lobes with respect to the polarization axes suggesting that crystalline domains of spherulitic morphologies are formed in the case of **5**,[30] while during cooling an isotropic melt of **3c**, supramolecular aggregates of elongated shape develop.[31] The change in the morphologies between **5** and **3c** may be assigned to the difference in backbones stiffness, that is enhanced by the incorporation of ethynylene moieties, giving rise to formation of rodlike aggregates. SALS experiments performed for **7a** did not allow us to elucidate the developed morphology.

Absorption and Photoluminescence Studies. The investigations of the absorption and photoluminescence properties of the polymers were carried out in dilute chloroform solution as well as in solid films. The thin films of 100−150 nm thickness of the sample and the reference polymer were spin casted from chlorobenzene solutions.[22] For the purpose of reproducibility of the photophysical data, two films of each sample were measured. Photoluminescence data were obtained upon excitation at the wavelength of the absorption maximum. The absorption peak maxima, λ_a, the extinction coefficients at the peak maxima, ϵ_{max}, the wavelength at which the extinction has dropped to 10% of the peak value, $\lambda_{10\%max}$,[23b] and the optical band gap energy, E_g^{opt} (obtained from $\lambda_{10\%max}$), are presented in Table 1. Data from the photoluminescence studies, namely the excitation wavelength, λ_{ex}, the emission maxima, λ_e, the Stokes shift, the full width at half-maximum of the emission, $fwhm_e$, and the fluorescence quantum yields, ϕ_{fl}, are summarized in Table 2. Figures 4 and 5 show the absorption and emission spectra respectively in chloroform solution and in solid state. For the purpose of comparison and a better elucidation of the observed optical and electrochemical data (see below) it was essential to include the data of polymers **3d**[21a,22a] and

Table 1. UV−Vis Data in Dilute Chloroform Solution and in the Solid State

code	λ_a (nm)	ϵ_{max}[c] ($M^{-1}\,cm^{-1}$)	$\lambda_{10\%max}$ (nm)	E_g^{opt}[d] (eV)
3b[a]	427	91100	484	2.56
3b[b]	454		534	2.32
3c[a]	443	77000	490	2.52
3c[b]	*452*, 479.5		510	2.43
3d[b]	465		519	2.39
5[a]	460	29300	542	2.28
5[b]	495		603	2.05
7a[a]	456	50400	523	2.37
7a[b]	475		554	2.24
7b[a]	477	73700	528	2.34
7b[b]	491		570	2.17

[a] Solution. [b] Solid state. [c] Per mole of the constitutional unit. [d] $E_g^{opt} = hc/\lambda_{10\%max}$.

Table 2. Photoluminescence Data in Dilute Chloroform Solution and in the Solid State

code	λ_{ex} (nm)	λ_e (nm)	Stokes shift (nm)	fwhm$_e$ (cm^{-1})	ϕ_{fl} (%)
3b[a]	430	494	67	2500	20
3b[b]	456	574	120	3600	56
3c[a]	446	489	46	2000	100
3c[b]	454	507, *540*	88	3200	35
3d[b]	465	602	137	4900	19
5[a]	460	556	96	2300	40
5[b]	495	642	147	2800	54
7a[a]	460	536	80	2600	12
7a[b]	473	616	141	3500	50
7b[a]	476	525	48	1400	80
7b[b]	491	*556*, 593	65	2380	19

[a] Solution. [b] Solid state.

7b[24d] (Scheme 1), whose syntheses have been reported elsewhere. The solid-state absorption and emission spectra of **7b** are shown in the Supporting Information, Figure S3.

The solution absorption maximum of the CN-containing polymer **3b** (λ_a = 427 nm, E_g^{opt} = 2.56 eV) is approximately 20 nm blue shifted to that of its CN-free counterpart **3c** (λ_a = 443 nm, E_g^{opt} = 2.52 eV). In the solid state, the reverse situation occurs. Although both polymers show almost similar absorption maxima around 452−454 nm, the solid-state optical band gap energy of **3b** (E_g^{opt} = 2.32 eV) is 0.11 eV lower than that of **3c** (E_g^{opt} = 2.43 eV). Accordingly, the colors of the bulk samples are different, i.e., bright orange for **3b** and yellow for **3c**. This can be interpretated as being due to relatively strong aggregate formation in the case of **3b** as indicated by the strong tailing of the solid-state absorption spectrum. The absorption of the CN-free polymer **7b** in solution (λ_a = 477 nm, E_g^{opt} = 2.34 eV) as well as in the solid state (λ_a = 491 nm, E_g^{opt} = 2.17 eV)[24d] is significantly red shifted compared to that of its CN-containing partner **7a** (solution λ_a = 456 nm, E_g^{opt} = 2.37 eV; solid λ_a = 475 nm, E_g^{opt} = 2.24 eV).

All the emission spectra of the CN-containing polymers **3b** (solution λ_e = 494 nm; solid λ_e = 574 nm) and **7a** (solution λ_e = 536 nm; solid λ_e = 616 nm) are red shifted compared with those of their respective CN-free counterparts **3c** (solution λ_e = 489 nm; solid λ_e = 507, 540 nm) and **7b**. The absence of triple bonds in the backbone of the fully substituted polymer **5** explains the bathochromic shift of its absorption (solution λ_e = 460 nm, E_g^{opt} = 2.28 eV; solid λ_e = 495 nm, E_g^{opt} = 2.05 eV) and emission spectra (solution λ_e = 556 nm; solid λ_e = 642 nm) compared to the fully substituted ethynylene-containing polymer **7a**. In the visible range between 400 and 700 nm, only single absorption and emission peaks appear in the case of the CN-containing polymers, indicating the lack of vibronic transitions, which are existent in the cases of CN-free **3c** and **7b**. The absence of vibronic transition would suggest the existence of significant ring distortion in the main chain, which probably originates from the addition of the bulky cyano group on the vinylene unit, as has been previously reported on other alkoxy-substituted CN−PPVs by Chen and Chang[15b] and others.[17b]

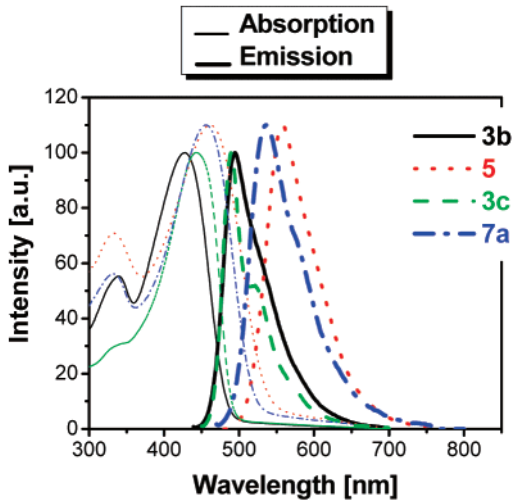

Figure 4. Normalized absorption and emission spectra of polymers **3b**, **3c**, **5**, and **7a** in dilute chloroform solution.

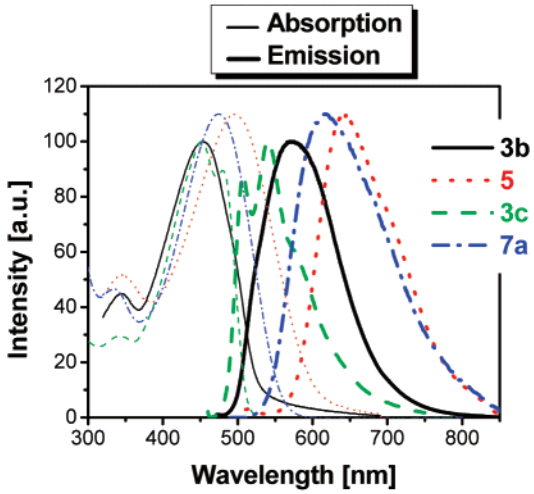

Figure 5. Normalized solid-state absorption and emission spectra of polymers **3b**, **3c**, **5**, and **7a**.

All the CN-containing polymers exhibit lower solution fluorescence quantum yields (12−40%) than their CN-free counterparts (80−100%), probably due to the above-mentioned noncoplanarity of the main chain. Their solid state fluorescence quantum yields are on the contrary higher (50−60 %), probably resulting from the combination of enhanced coplanarity of the polymers backbone (relative to the solution) and lack of significant excimer-like quenching process. This moreover confirms the trend observed in other CN−PPVs.[14b,15c] For example, Greenham et al. reported a solid-state fluorescence quantum yield of 48% for MEH−CN−PPV.[14b] This is in contrast to most CN-free polymers, which usually exhibit higher fluorescence quantum yields in solution than in solid state, e.g., polymer **3c**.

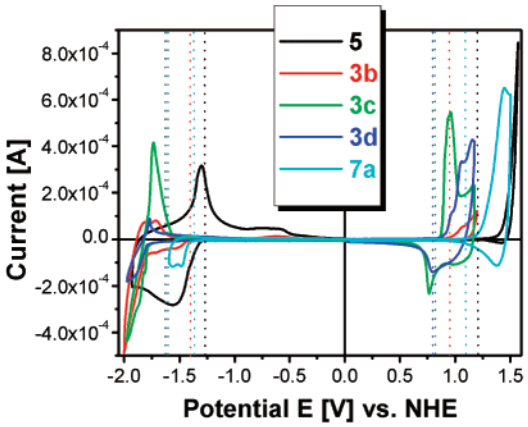

Figure 6. CV-curves of polymers **3b**, **3c**, **3d**, **5**, and **7a.** The vertical lines show the redox onset values as obtained by EVS.

Table 3. Electrochemical Data of Polymers 3b, 3c, 3d, 5, 7a, and 7b as Obtained from Cyclic Voltammetry and Electrochemical Voltage Spectroscopy[a]

code	E_{onset}^{ox} (mV)	E_{onset}^{red} (mV)	HOMO (eV)	LUMO (eV)	E_g^{ec} (eV)	$E_g^{ec} - E_g^{opt}$ (eV)
3b	+950	−1400	−5.7	−3.35	2.35	0.03
3c	+815	−1615	−5.56	−3.13	2.43	0.00
3d	+795	−1620	−5.54	−3.13	2.41	0.02
5	+1220	−1270	−5.97	−3.48	2.49	0.44
7a	+1090	−1370	−5.84	−3.38	2.46	0.22
7b	+565	−1725	−5.32	−3.03	2.29	0.12

[a] All potentials are given vs the normal hydrogen electrode (NHE).[27] The NHE level used for the HOMO−LUMO calculation was −4.75 eV.

Electrochemical Studies. The electrochemical behavior of the polymers was investigated by the combination of cyclic voltammetry (CV) and electrochemical voltage spectroscopy (EVS). CV and EVS were performed in a solution of Bu_4NClO_4 (98%, ∼0.1 M) in anhydrous acetonitrile at a scan rate of 10 mV/s. A platinum electrode coated with a thin polymer film was used as the working electrode. A Pt foil served as the counterelectrode and an Ag/AgCl electrode was used as the reference electrode.

Figure 6 gives the CV curves of **3b**, **3c**, **3d**, **5**, and **7a**. The vertical lines show the redox onset values as obtained through EVS. The electrochemical data of the polymers are given in Table 3. All the potential values shown are vs normal hydrogen electrode (NHE). The NHE level in the Fermi scale used for HOMO−LUMO calculation was −4.75 eV.[27,32−33]

The reduction process in both **3b** and **5** was partially reversible; whereas the oxidation process was irreversible. Both p- and n-doping processes were irreversible in the case of **7a**. Such irreversibility in the electrochemical processes has been reported for several alkoxy-substituted π-conjugated polymers[34,35] and has been attributed to a strong interaction of the anion dopant (ClO_4^- in the present situation) with the alkoxy side chain. Reversible redox curves were obtained for CN-free polymers **3c**, **3d**, and **7b**.[24d]

A comparison of the optical, E_g^{opt}, and electrochemical, E_g^{ec} band gap energies (Table 3, last column) reveals following results: (a) Polymers **3b**, **3c**, and **3d**, having in common two −C≡C− moieties per repeating unit and comparatively less side chains, show identical E_g^{opt} and E_g^{ec} values. The discrepancy (ΔE_g) of both values lies within the range of error. (b) The fully substituted polymers, whose constitutional units include either one

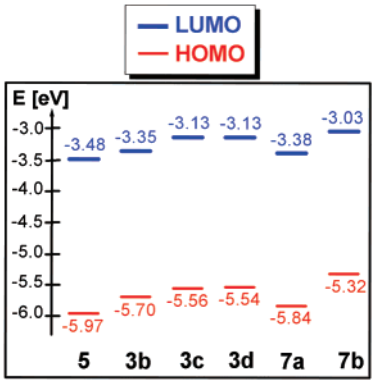

Figure 7. Position of the HOMO and LUMO of the polymers **3b**, **3c**, **3d**, **5**, **7a**, and **7b** in the Fermi energy scale.

(**7a** and **7b**) or no −C≡C− units (**5**), show a significant difference between E_g^{opt} and E_g^{ec}. This discrepancy increases from the CN-free polymer **7b** (0.12 eV) through the CN- and ethynylene-containing polymer **7a** (0.22 eV) to the ethynlene-free and CN-containing compound **5** (0.44 eV) suggesting a clear correlation between the backbone rigidity (i.e., coplanarity) and ΔE_g.

The above results might be interpreted in terms of differences or similarities in the polymer chains alignment (i.e., morphology) in films prepared by *spin coating* for optical investigations and by *drop casting* for the electrochemical studies. In the case of polymers **3b**, **3c**, and **3d**,[21a] with intrinsic self-assembly ability, the film preparation methods might have very little effect on the film morphology, which would explain the similarity in both E_g^{opt} and E_g^{ec} values. The intrinsic self-assembly ability in **3c** and **3d** moreover would explain the color differences found in the bulk of both materials. The orange color of **3d** and its concomitant lower optical band gap energy (compared to **3c**) are clear indications of enhanced planarisation of the conjugated backbone due to a specific orientation and self-assembly of the polymeric chains, attributed to the grafting of octadecyloxy side groups on the phenylene−ethynylene segment and octyloxy side groups on the phenylene−vinylene segment of the polymer.[28] In the case of the fully substituted and less rigid polymers **7a** and **7b** and in particular the dodecyloxy-substituted ethynylene-free and CN-containing polymer **5**, a dependence of the film morphology on the preparation methods (i.e., different average effective conjugated lengths are created due to various degree of distortion of the polymer backbone caused by steric hindrances originating from the higher density of side chains in combination with the presence of CN units in the cases of **5** and **7a**) would be expected, as has been clearly demonstrated by Chen et al.,[15b] Heeger et al.,[36] Barnes et al., and others.[37] This might explain the discrepancy of their both band gap values. Another explanation could be the higher density combined with the length of grafted side chains, which might play the role of a *shield* of the conjugated backbone during the n- and p-doping processes in the electrochemical study. This second tentative explanation is supported by our previous findings on polymers of the type of **7b**, where bulky or longer side chains led to an increase ΔE_g.[24d]

It is obvious from Figure 7 and from Table 3 that the incorporation of CN units in the backbone of **3b** and **7a** lowers their HOMO level respectively by 140 and 520 meV and their LUMO level by 220 and 350 meV compared with their corresponding CN-free counter-

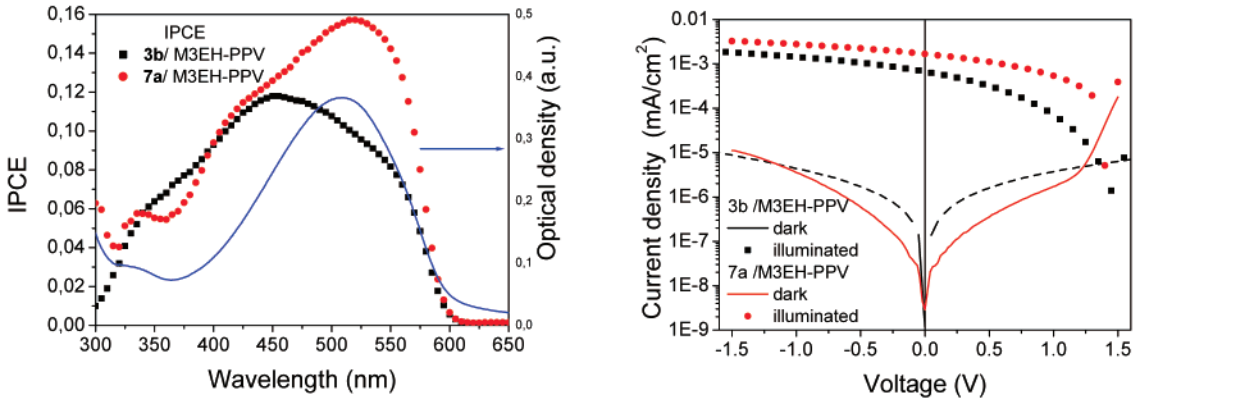

Figure 8. Solar cell characteristics of devices with blend (ratio 1:1) layers comprised of **3b**:M3EH−PPV and **7b**:M3EH−PPV. Left: External quantum efficiency (IPCE) of the devices and absorbance of M3EH−PPV (solid line). Right: $I(V)$ characteristics in the dark and under white light illumination with 100 mW/cm^2).

parts **3c** and **7b**, clearly suggesting an improvement in the electron-accepting strength, despite the above-mentioned discrepancy situation in the case of **7a**.

Photovoltaic Studies. It is well-known that solar cells containing a heterojunction between two different polymers, with one acting as the hole acceptor and the other as an electron acceptor, show much better performances than single component devices.[5,38−39] Photogenerated excitons in the polymer layer can be efficiently dissociated into free carriers at the interface between the electron-donating and the electron-accepting polymers. This heterojunction can be introduced either by preparing double layer devices or by blending the two polymers, yielding a distributed bulk heterojunction. Solar cells in which the active layer is prepared from a polymer blend have the advantage of a larger interfacial area. However, to extract the photogenerated charges from the device, the blend morphology must contain percolating paths to the electrodes for both kinds of carriers.[40] In addition, since the entropy of mixing of polymers is relatively low, mixtures of polymers deposited from organic solvents tend to phase separate during the evaporation of the solvent, resulting in a coarse grain morphology. The advantage of double layer devices is that once the excitons are separated, there exists always a direct path for both carriers to travel to the corresponding electrodes. However, in general, double layer devices are more difficult to prepare since they require either perpendicular solubility of the polymers in different solvents or cross-linking of the first layer to prevent that the first layer is washed away when the second layer is deposited. An alternative approach is to use a lamination technique which is, however, rather unsuitable for large area production.[41] We decided to use the alternating copolymer poly[2,5-dimethoxy-1,4-phenylene−vinylene-2-methoxy-5-(2-ethylhexyloxy)-1,4-phenylene−vinylene] (M3EH−PPV)[42] (for the chemical structure see the Supporting Information, Figure S4) as electron donator for the photovoltaic studies together with the electron acceptors **3b**, **5**, and **7a**, since, with this choice, double layer as well as blend devices could be prepared. M3EH−PPV shows a good solubility in polar solvents like chlorobenzene but a very low solubility in less polar solvents like *p*-xylene. Thus, it is possible to construct a double layer device by spin-coating the electron-accepting polymers **3b**, **5**, and **7a** dissolved in *p*-xylene on top of a M3EH−PPV layer.

In the first step, single layer devices of **3b**, **3c**, **7a**, and **7b** as well as blend devices of **3b** or **7a** as electron acceptor together with M3EH−PPV as electron donator in a ratio of 1:1 were prepared as described in the Supporting Information. As expected, the efficiencies for single layer cells are quite low. However, the devices containing polymers with only one triple bond in the repeating unit, **7a** and **7b**, show with 2.2% and 3.9%, respectively, a surprising high external quantum efficiency (IPCE). On the contrary, pure single layer devices with **3b**, **3c**, and **5** reach only a peak IPCE of 0.35%, 0.15%, and 0.9% respectively.

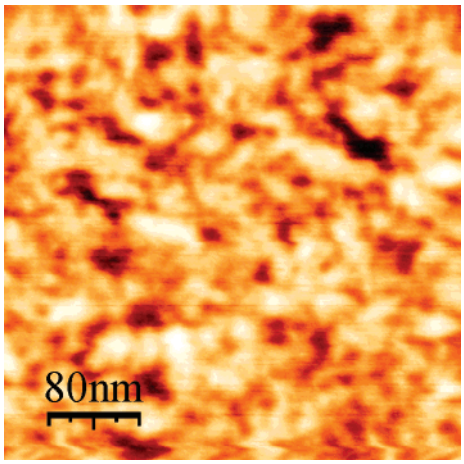

Figure 9. Atomic force microscopy (AFM) phase contrast image of a film consisting of a M3EH−PPV:**3b** 1:1 blend.

For the blend devices the external quantum efficiencies and the current−voltage characteristics under white light illumination at 100 mW/cm^2 are shown in Figure 8. These blend devices exhibit a large IPCE of up to 11% for **3b** and 16% for **7a**. Under white light illumination, the open circuit voltage is as large as 1.43V for **3b** and 1.40V for **7a**. Both blend devices differ fundamentally in the shape of the $I(V)$ characteristics. The **3b**:M3EH−PPV solar cell shows a surprising small fill factor of only 16%, whereas the fill factor of 26% for the **7a**:M3EH−PPV cell is within typical values obtained for polymer blends. As a result, the energy efficiencies under white light are 0.16% and 0.62% for **3b** and **7a** respectively. A possible large scale phase separation for the **3b**:M3EH−PPV device can be excluded as a reason for the low efficiency. As shown by the AFM picture in Figure 9, the **3b**:M3EH−PPV blend layer exhibits a fine phase-separated structure with a domain size smaller than 40 nm.

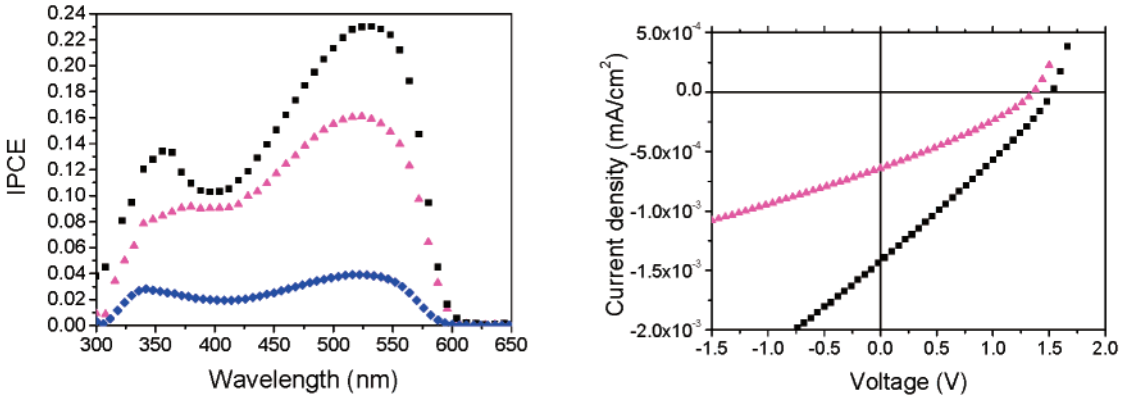

Figure 10. Left: External quantum efficiency for the single M3EH−PPV layer (diamonds), a M3EH−PPV:**5** bilayer structure (triangles) and a M3EH−PPV:**3b** bilayer (squares). Right: *I*(*V*) characteristics of a M3EH−PPV:**5** bilayer structure (triangles) and a M3EH−PPV:**3b** bilayer device (squares). The layer thicknesses were 30 nm for the M3EH−PPV layer and 10 nm for the electron transporting layer.

The rather low fill factor for the **3b**:M3EH−PPV blend and the very low efficiency in the **3b** single layer device suggest that a large fraction of the photogenerated charge carriers recombine before reaching the corresponding electrodes. One possible reason is that the phase-separated morphology prevents most photogenerated carriers to reach the external circuit. Therefore, we have compared the performance of the blend diodes with that of bilayer devices prepared from the same polymers. It was found that the efficiencies are very sensitive to the thicknesses of both layers. In general, thicker layer will absorb more light and, consequently, more excitons are generated. On the other hand, due to the small exciton diffusion length in polymers, only a fraction of excitons will reach the interface and dissociate into free carriers. In addition, if the charge carrier mobility in one (or both) polymer components is low, increasing the layer thickness will result in a larger voltage drop across the layer, resulting in a smaller fill factor. This effect might explain the different performance of bilayer devices using either **3b** or **5** as shown in Figure 10. Apparently, the photoactive spectrum is dominated by light absorbed in the M3EH−PPV layer. This is meaningful, since the illumination is through the transparent anode adjacent to the M3EH−PPV layer and because the electron-conducting layer in these devices is rather thin (ca. 10 nm).

Nevertheless, the two devices differ significantly with respect to efficiency and fill factor. With an optimum **3b** layer thickness of 10 nm the peak external quantum efficiency is as high as 23% (Figure 10). This is more than 5 times higher than that of a corresponding single layer M3EH−PPV device with the same PPV layer thickness. Also, the peak IPCE efficiency of the M3EH−PPV:**3b** device is significantly larger than that of the **5** bilayer device (with the same thickness of the electron-accepting polymer). Moreover, the bilayer solar cell containing **3b** exhibits an open circuit voltage as high as 1.52 V, nearly independent of the layer thicknesses, compared to only 1.38 V in the case of **5**. For **7a**, the external quantum efficiency reaches the same value as for the blend device.

From literature values the HOMO energy of M3EH−PPV was calculated to −5.45 eV and the LUMO energy to −3.06 eV. Thus, the band offsets between the acceptor polymers and M3EH−PPV are in sum 340 meV smaller for **3b** than for **5**. This explains the larger open circuit voltage measured for the M3EH−PPV:**3b** solar cell.

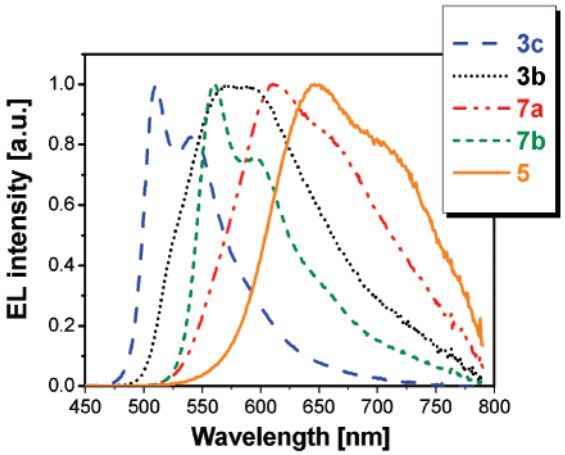

Figure 11. Electroluminescence spectra of **3b**, **3c**, **5**, **7a**, and **7b** from ITO/PEDOT:PSS/polymer/Ca/Al devices.

The results indicate that **3b** and **7a** act as efficient electron acceptors. On the other hand, the small fill factors of 26.5% of the bilayer and only 16% in the blend device with **3b** suggest that the transport of electrons in **3b** is inefficient. Together with quantum efficiency data obtained for the single layer devices, it can be suggested that introducing two triple bonds decreases the transport properties, at least for the electrons. This interpretation is supported by the observation that the fill factor decreases further with increasing **3b** layer thickness to below 20%. Alternatively, a barrier for electron extraction to the Ca cathode might account for the strong dependence of the photocurrent on the applied voltage. Further studies on the electron mobility in **3b** in comparison to **5** are necessary to understand and finally address this point. Despite the small fill factor, the overall power efficiency of the **3b** containing device is 0.65% (compared to 0.35% for the **5** bilayer device), which is one of the highest value reported for pure polymer-blend solar cells.[43] Finally, note that the fill factor of the M3EH−PPV:**3b** bilayer device is significantly larger than that of the corresponding blend device. This suggests further losses by insufficient electron transport and recombination in the interpenetrating network of the blend layers.

Electroluminescent Properties. In Figure 11, the EL spectra of ITO/PEDOT:PSS/polymer/Ca/Al LEDs using the polymers **3b**, **3c**, **5**, **7a**, and **7b** are shown. The device made from polymer **3c** emits green light at

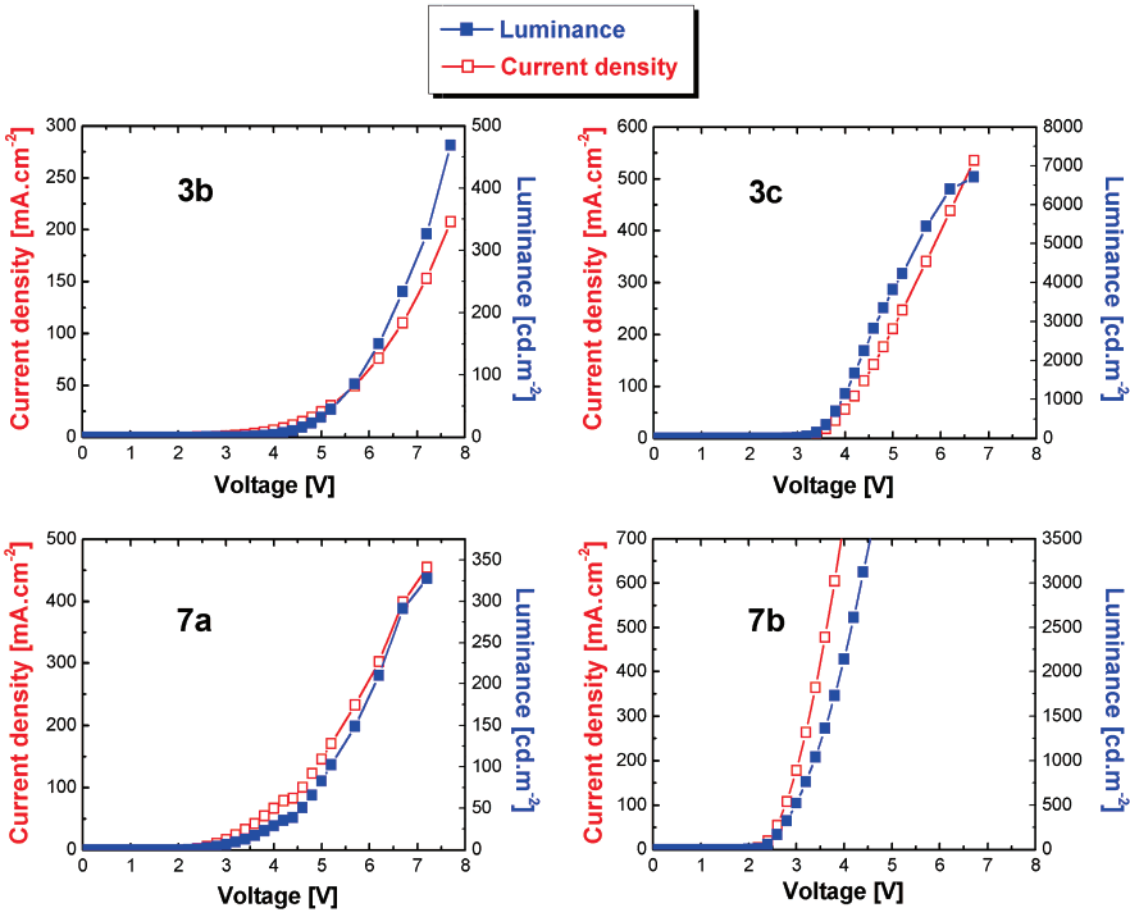

Figure 12. Current density−voltage (□) and luminance−voltage (■) characteristics for ITO/PEDOT:PSS/polymer/Ca/Al devices from polymers **3b**, **3c**, **5**, **7a**, and **7b**.

Table 4. Electroluminescence Data of Polymers 3b, 3c, 5, 7a, and 7b from ITO/PEDOT:PSS/Polymer/Ca/Al Devices

code	λ_{El} (nm)	luminance (cd/m^2) at 100 mA/cm^2	CIE color coordinates (X, Y)	max efficiency (cd/A)
3b	582	170	(0.497, 0.496)	0.23
3c	510	1300	(0.358, 0.593)	2.05
5	648	1.5	(0.633, 0.366)	0.02
7a	612	51	(0.594, 0.406)	0.07
7b	559	310	(0.521, 0.479)	0.3

510 nm. The other devices emit in the red region at 559 (**7b**), 582 (**3b**), 612 (**7a**), and 648 nm (**5**). Similar to the PL spectra, only EL spectra from CN-free polymers **3c** and **7b** show two well resolved bands corresponding to the 0−0 and 0−1 vibrational transitions. Figure 12 shows the current density and luminance vs voltage characteristics for the LEDs of **3b**, **3c**, **7a**, and **7b**. Their efficiency-voltage characteristics are depicted in the Supporting Information, Figure S5. Supporting Information Figure S6 shows the current density, the luminance and the efficiency vs voltage for the LED device from polymer **5**. In common for all devices are the low turn-on voltages below 3 V. The lowest turn-on voltage is found at 2.0 V for the device containing **7b**. The turn-on voltages for **3c**, **5**, and **7a** are 2.2 V and for **3b** the voltage is 2.5 V**.** The brightest LED with an efficiency of more than 2 cd/A is based on **3c** followed by **7b** (0.3 cd/A) (Table 4), indicating a better EL performance for the CN-free polymers than their CN-containing counterparts.

Conclusions

Alkoxy-substituted CN-containing phenylene−vinylene-*alt*-phenylene−ethynylene hybrid polymers **3a**, **3b**, and **7a** have been synthesized by the Knoevenagel reaction of luminophoric dialdehydes **1** or **6** with the dinitrile **2a**. CN-free phenylene−ethynylene-*alt*-phenylene−vinylene polymers **3c**, **3d**, and **7b** and an ethynylene-free CN-phenylene−vinylene polymer **5** were considered for the purpose of comparison. CN-containing polymers **3b**, **5**, and **7a** exhibit higher fluorescence quantum yields in solid state than in solution in contrast to CN-free polymers. The incorporation of the CN units within the backbone of **3b** and **7a** enhances their electron accepting strength compared to their respective CN-free counterparts **3c** and **7b**. A correlation between level of backbone stiffness (and coplanarity) combined with nature and number of side chains and the discrepancy ΔE_g could be established. Moreover, high external quantum efficiencies of up to 23%, an open circuit voltage of up to 1.52 V, and a white light energy efficiency of 0.65% were realized in bilayer solar cell devices with a PPV-based electron-donating polymer and **3b** as acceptor. However, the rather low fill factor of these solar cells suggests that the electron mobility in these hybrid polymers is rather low. One possible reason for this finding is that due to the presence of the triple bonds, rotation of adjacent phenyl rings with respect to each other has a low energetic barrier of rotation.[44] It is known that the HOMO and LUMO energies of poly(*p*-phenyleneethynylene)s depend on the dihedral angle between adjacent benzene rings.[45] We, therefore, presume that this free-

dom of rotation results in a wider distribution of transport site energies when compared to the corresponding ethynylene-free materials. Thus, further synthetic efforts are on the way with the focus to design novel polymers with superior electron-accepting and electron-transporting properties. LED devices from **3b**, **3c**, **7a**, and **7b** of configuration ITO/PEDOT:PSS/polymer/Ca/Al showed low turn-on voltage between 2 and 2.5 V. The EL parameters of CN-free polymers **3c** and **7b** were far better than those of their respective CN-containing counterparts.

Acknowledgment. We are grateful to Dr. Eckhard Birckner, of the Institute of Physical Chemistry, Friedrich-Schiller University Jena, Jena, Germany, for carrying out the photoluminescence investigations in solution. We further acknowledge financial support by the Volkswagen Foundation and the Fond der chemischen Industrie.

Supporting Information Available: Text describing the experimental procedures and the the synthesis of the materials and figures showing the ^{13}C NMR spectrum of **5**, small-angle light scattering patterns of **5** and **3c**, normalized solid state absorption and emmission of **7b**, the chemical structure of M3EH−PPV, efficiency−voltage characteristics of **3b**, **3c**, **7a**, and **7b**, and current density−voltage, luminance−voltage, and efficiency−voltage characteristics of **5**. This material is available free of charge via the Internet at http://pubs.acs.org.

References and Notes

(1) Burroughes, J. H.; Bradley, D. D. C.; Brown, A. R.; Marks, R. N.; MacKays, K.; Friend, R. H.; Burn, P. L.; Holmes, A. B. *Nature (London)* **1990**, *347*, 539.
(2) Sariciftci, N. S.; Smilowitz, L.; Heeger, A. J.; Wudl, F. *Science* **1992**, *258*, 1789.
(3) Brabec, C. J.; Zerza, G.; Cerullo, G.; De Silvestri, S.; Luzzati, S.; Hummelen, J. C.; Sariciftci, N. S. *Chem. Phys. Lett.* **2001**, *340*, 232.
(4) Montari, I.; Nogueira, A. F.; Nelson, J.; Durrant, J. R.; Winder, C.; Loi, M. A.; Sariciftci, N. S.; Brabec, C. J. *Appl. Phys. Lett.* **2002**, *81*, 3001.
(5) Brabec, C. J.; Sariciftci, N. S.; Hummelen, J. C. *Adv. Funct. Mater.* **2001**, *11*, 15.
(6) (a) Winder, C.; Sariciftci, N. S. *J. Mater. Chem.* **2004**, *14*, 1077. (b) van Duren, J. K. J.; Yang, X.; Loos, J.; Bulle-Lieuwma, C. W. T.; Sieval, A. B.; Hummelen, J. C.; Janssen, R. A. J. *Proc. SPIE* **2004**, *5215*, 99.
(7) Hadziioannou, G., van Hutten, P. F., Eds. *Semiconducting Polymers: Chemistry, Physics and Engineering*, 1st ed.; Wiley-VCH: Weinheim, Germany, 2000.
(8) Kraft, A.; Grimsdale, A. C.; Holmes, A. B. *Angew. Chem.* **1998**, *110*, 416.
(9) Breeze, A. J.; Schlesinger, Z.; Carter, S. A.; Hörhold, H.-H.; Tillmann, H.; Ginley, D. S.; Brock, P. J. *Proc. SPIE* **2001**, *4108*, 57.
(10) Koetse, M. M.; Sweelsen, J.; Franse, T.; Veenstra, S. C.; Kroon, J. M.; Yang, X.; Alexeev, A.; Loos, J.; Schubert, U. S.; Schoo, H. F. M. *Proc. SPIE* **2004**, *5215*, 119.
(11) (a) Cacialli, F.; Marks, R. N.; Friend, R. H.; Zamboni, R.; Taliani, C.; Moratti, S. C.; Holmes, A. B. *Synth. Met.* **1996**, *76*, 148. (b) Peng, Z.; Galvin, M. E. *Chem. Mater.* **1998**, *10*, 1785. (c) Tada, K.; Hosoda, K.; Hirohata, M.; Hidayat, R.; Kawai, T.; Onoda, M.; Teraguchi, M.; Masuda, T.; Zakhidov, A. A.; Yoshino, K. *Synth. Met.* **1997**, *85*, 1305.
(12) Gillissen, S.; Jonforsen, M.; Kesters, E.; Johansson, T.; Theander, M.; Andersson, M. R.; Inganäs, O.; Lutsen, L.; Vanderzande, D. *Macromolecules* **2001**, *34*, 7294 and references therein.
(13) (a) Greenham, N. C.; Moratti, S. C.; Bradley, D. D. C.; Friend, R. H.; Holmes, A. B. *Nature (London)* **1993**, *365*, 628. (b) Samuel, I. D. W.; Rumbles, G.; Collison, C. J. *Phys. Rev. B* **1995**, *52*, 573.
(14) (a) Moratti, S. C.; Cervini, R.; Holmes, A. B.; Baigent, D. R.; Friend, R. H.; Greenham, N. C.; Grüner, J.; Hamer, P. J. *Synth. Met.* **1995**, *71*, 2117. (b) Greenham, N. C.; Samuel, I. D. W.; Hayes, G. R.; Phillips, R. T.; Kessener, Y. A. R. R.; Moratti, S. C.; Holmes, A. B.; Friend, R. H. *Chem. Phys. Lett.* **1995**, *241*, 89.
(15) (a) Gill, R. E.; van Hutten, P. F.; Meetsma, A.; Hadziioannou, G. *Chem. Mater.* **1996**, *8*, 1341. (b) Chen, S.-A.; Chang, E.-C. *Macromolecules* **1998**, *31*, 4899. (c) Tillmann, H.; Hörhold, H.-H. *Synth. Met.* **1999**, *101*, 138.
(16) (a) Behnisch, B.; Martinez-Ruiz, P.; Schweikart, K.-H.; Hanack, M. *Eur. J. Org. Chem.* **2000**, *14*, 2541. (b) Mitschke, U.; Bäuerle, P. *J. Mater. Chem.* **2000**, *10*, 1471 and references therein.
(17) (a) Jin, Y.; Ju, J.; Kim, J.; Lee, S.; Kim, J. Y.; Park, S. H.; Son, S.-M.; Jin, S.-H.; Lee, K.; Suh, H. *Macromolecules* **2003**, *36*, 6970. (b) Fang, Q.; Jiang, B.; Xu, B.; Wang, W.; Yu, F.; Wu, X. *Macromol. Rapid Commun.*. **2004**, *25*, 1429.
(18) Pinto, M. R.; Hu, B.; Karasz, F. E.; Akcelrud, L. *Polymer* **2000**, *41*, 2603.
(19) Liu, M. S.; Jiang, X.; Liu, S.; Herguth, P.; Jen, A. K. Y. *Macromolecules* **2002**, *35*, 3532.
(20) (a) Brizius, G.; Pschirer, N. G.; Steffen, W.; Stitzer, K.; zur Loye, H.-C.; Bunz, U. H. F. *J. Am. Chem. Soc.* **2000**, *122*, 12435. (b) Bunz, U. H. F. *Acc. Chem. Res.* **2001**, *34*, 998.
(21) (a) Egbe, D. A. M.; Tillmann, H.; Birckner, E.; Klemm, E. *Macromol. Chem. Phys.* **2001**, *202*, 2712. (b) Ramos, A. M.; Rispens, M. T.; van Duren, J. K. J.; Hummelen, J. C.; Janssen, R. A. J. *J. Am. Chem. Soc.* **2001.** *123*, 6714.
(22) (a) Egbe, D. A. M.; Roll, C. P.; Birckner, E.; Grummt, U.-W.; Stockmann, R.; Klemm, E. *Macromolecules* **2002**, *35*, 3825. (b) Egbe, D. A. M.; Roll, C. P.; Klemm, E. *Des. Monomers Polym.* **2002**, *5*, 245. (c) Egbe, D. A. M.; Birckner, E.; Klemm, E. *J. Polym. Sci., Part A: Polym. Chem.* **2002**, *40*, 2670. (d) Wilson, J. N.; Windscheif, P. M.; Evans, U.; Myrick, M. L.; Bunz, U. H. F. *Macromolecules* **2002**, *35*, 8681.
(23) (a) Chu, Q.; Pang, Y.; Ding, L.; Karasz, F. E. *Macromolecules* **2003**, *36*, 3848. (b) Egbe, D. A. M.; Bader, C.; Nowotny, J.; Günther, W.; Klemm, E. *Macromolecules* **2003**, *36*, 5459. (c) Egbe, D. A. M.; Bader, C.; Klemm, E.; Ding, L.; Karasz, F. E.; Grummt, U.-W.; Birckner, E. *Macromolecules* **2003**, *36*, 9303. (d) Zhokhavets, U.; Goldhahn, R.; Gobsch, G.; Al-Ibrahim, M.; Roth, H.-K.; Sensfuss, S.; Klemm, E.; Egbe, D. A. M. *Thin Solid Films* **2003**, *444*, 215.
(24) (a) Egbe, D. A. M.; Stockmann, R.; Hotzel, *M. J. Opt. A: Pure Appl. Opt.* **2004**, *6*, 791. (b) Tong, M.; Sheng, C. X.; Yang, C.; Vardeny, Z. V. *Phys. Rev. B* **2004**, *69*, 155211. (c) Ding, L. Egbe, D. A. M.; Karasz, F. E. *Macromolecules* **2004**, *37*, 6124. (d) Egbe, D. A. M.; Carbonnier, B.; Ding, L.; Mühlbacher, D.; Birckner, E.; Pakula, T.; Karasz, F. E.; Grummt, U.-W. *Macromolecules* **2004**, *37*, 7451.
(25) (a) Kaufman, J. H.; Chung, T.-C.; Heeger, A. J. *Solid State Commun.* **1983**, *47*, 585. (b) Kaufman, J. H.; Chung, T.-C.; Heeger, A. J. *J. Electrochem. Soc.* **1984**, *131*, 2847. (c) Kaner, R. B.; Porter, S. J.; Nairns, D. P.; MacDiarmid, A. G. *J. Chem. Phys.* **1989**, *90*, 1303.
(26) (a) Thompson, A. H. *Phys. Rev. Lett.* **1978**, *40*, 1511. (b) Thompson, A. H. *J. Electrochem. Soc.* **1979**, *126*, 608. (c) Thompson, A. H. *Rev. Sci. Instrum.* **1983**, *54*, 229.
(27) Mühlbacher, D. Diploma Thesis. Johann Kepler University Linz, Austria 2002.
(28) Egbe, D. A. M.; Roll, Bader, C.; Nowotny, J.; Klemm, E. *Proc. SPIE* **2004**, *5215*, 79.
(29) Chen, Z.-K.; Meng, H.; Lai, Y.-H.; Huang, W. *Macromolecules* **1999**, *32*, 4351.
(30) (a) Stein, R. S.; Rhodes, M. B. *J. Appl. Phys.* **1960**, *31*, 1873. (b) Stein, R. S. In *Structures and Properties of Polymer Films*; Lenz, R. W., Stein, R. S., Eds.; Plenum: New York, 1973. (c) Samuels, R. J. *J. Polym. Sci., Part A-2* **1971**, *9*, 2165.
(31) Stein, R. S.; Erhardt, P.; van Aartsen, J. J.; Clough, S.; Rhodes, M. *J. Polym. Sci., Part C* **1966**, *13*, 1.
(32) Gomer, R. J.; Tryson, G. *J. Chem. Phys.* **1977**, *66*, 4413.
(33) Kötz, R.; Neff, H.; Müller, K. *J. Electroanal. Chem.* **1986**, *215*, 331.
(34) (a) Schiavon, G.; Zotti, G.; Bontempelli, G. *J. Electronal. Chem.* **1984**, *161*, 323. (b) Shiraishi, K.; Yamamoto, T. *Synth. Met.* **2002**, *130*, 139. (c) Yamamoto, T.; Etori, H. *Macromolecules* **1995**, *28*, 3378.
(35) (a) Yamamoto, T.; Fang, Q.; Morikita, T. *Macromolecules* **2003**, *36*, 4262. (b) Fang, Q. Yamamoto, T. *Macromolecules* **2004**, *37*, 5894.
(36) McGehee, M. D.; Heeger, A. J. *Adv. Mater.* **2000**, *12*, 1655 and references therein.

(37) Kumar, P.; Mehta, A.; Mahurin, S. M.; Dai, S.; Dadmun, M. D.; Sumpter, B. G.; Barnes, M. D. *Macromolecules* **2004**, *37*, 6132. and references therein.
(38) Yu, G.; Gao, J.; Hummelen, J. C.; Wudl, F.; Heeger, A. J. *Science* **1995**, *270*, 1789.
(39) Halls, J. J. M.; Walsh, C. A.; Greenham, N. C.; Marseglia, E. A.; Friend, R. H.; Moratti, S. C.; Holmes, A. B. *Nature (London)* **1995**, *376*, 498.
(40) van Duren,J. K. J.; Yang, X.; Loos, J.; Bulle-Lieuwma, C. W. T.; Sieval, A. B.; Hummelen, J. C.; Janssen, R. A. J. *Macromolecules* **2004**, *37*, 425.
(41) Granström, M.; Petrisch, K.; Arias, A. C.; Lux, A.; Anderson, M. R.; Friend, R. H *Nature (London)* **1998**, *395*, 257.
(42) Pfeiffer. S.; Hörhold, H.-H. *Macromol. Chem. Phys.* **1999**, *200*, 1870.
(43) Breeze, A. J.; Schlesinger, Z.; Carter, S. A.; Tillmann, H.; Hörhold, H.-H. *Solar Energy Mater. Solar Cells* **2004**, *83*, 263.
(44) (a) Okuyama, K.; Hasegawa, T.; Ito, M.; Mikami, N. *J. Phys. Chem.* **1984**, *88*, 1711. (b) Seminario, J. M.; Zacarias, A. G.; Tour, J. M. *J. Am. Chem. Soc.* **1998**, *120*, 3970.
(45) Miteva, T.; Kloppenburg, L.; Neher, D.; Bunz, U. H. F. *Macromolecules* **2000**, *33*, 6652.

MA048219B